Int. J. Electrochem. Sci., 15**(2020)** 4454 – 4469, doi: 10.20964/2020.05.45

International Journal of
ELECTROCHEMICAL
SCIENCE
www.electrochemsci.org

Influence of the Dissolved Oxygen Concentration in Artificial Seawater on the Corrosion Behavior of Q235 Mild Steel

P.R. Meng, Y. Chen, Z.L. Liu[*]

Department of Chemical Engineering and Safety, Binzhou University, Binzhou, Shandong 256600, China
[*]E-mail: liuzhilei98@126.com

Received: 21 December 2019/ *Accepted:* 27 January 2020 / *Published:* 10 April 2020

The corrosion behaviors of Q235 mild steel at different immersion times in artificial seawater containing different concentrations of dissolved oxygen were investigated using electrochemical impedance spectroscopy (EIS), electrochemical noise (EN) techniques and scanning electron microscopy (SEM). EIS results suggest that the sum of the charge transfer resistance and film resistance decreases with increasing immersion time and concentration of dissolved oxygen. A new electrochemical parameter C_{AE}, which represents the electrochemical reaction rate, is proposed and applied to evaluate the effect of dissolved oxygen concentration on the corrosion resistance and corrosion mechanism. The value of C_{AE} initially increases with immersion time and later decreases with prolonged testing time. The sum of the charge transfer resistance and film resistance shows the opposite variation trend with that of C_{AE} during the initial immersion times. Moreover, the observed morphologies of the Q235 mild steel surface agree well with the variation trend of C_{AE} at different dissolved oxygen concentrations. The above results reveal a new criterion to monitor the corrosion resistance and surface morphology in situ using an EN technique.

Keywords: mild steel; dissolved oxygen; artificial seawater; electrochemical noise

1. INTRODUCTION

Due to its excellent mechanical and engineering performance, Q235 mild steel is widely used as one of the most popular construction materials in the chemical, petroleum and marine engineering industries [1-3]. However, when placed in a seawater environment, the Q235 mild steel will be severely attacked. Compared with fresh water, the composition of seawater always features high concentrations of dissolved oxygen and high salinity, causing a much more severe corrosion of mild steel [4]. Thus, the investigation of the corrosion behavior of Q235 mild steel in ocean environments

has become significantly important, because remarkable corrosion may inevitably bring considerable economic and safety problems.

In previous studies, classic techniques, such as weight loss [5-7], potentiodynamic polarization [8,9], linear polarization [10], and electrochemical impedance spectroscopy (EIS) [11-13], have been employed to investigate the corrosion resistance and mechanism. Some useful parameters, such as corrosion potential, corrosion current density, and anodic and cathodic Tafel slopes, can be calculated using a Tafel extrapolation method during Tafel measurements to reveal the corrosion mechanism from both thermodynamic and dynamic aspects. Moreover, the polarization resistance is inversely related to the corrosion current density, where a large value corresponds to a low corrosion rate. Compared with the above techniques, an electrochemical noise (EN) technique serves as a more powerful and practical method to monitor the corrosion behavior without disturbing the corrosion system due to its nondestructive and nonintrusive nature [14-16]. Ashassi-Sorkhabi evaluated the anti-corrosive performance of epoxy-ZnO nanocomposite coatings using the EN technique in both the time and frequency domains and demonstrated that the resistance parameters obtained from both the EN and EIS techniques showed good agreement [17]. The corrosion resistance of Q235 mild steel in a seawater environment under static conditions depends mainly on the electrolyte composition, including the pH of the electrolyte, dissolved oxygen, Cl^- concentration and salinity [18]. Xue investigated the effect of chloride ion and dissolved oxygen concentrations on the corrosion behavior of low carbon steel in a 0.1 M $NaHCO_3$ solution and suggested that the corrosion of low carbon steel was accelerated under the synergistic effect of chloride ions and oxygen [19]. Moreover, the dissolved oxygen concentration displayed a much more remarkable effect on the average corrosion rate [20]. Unfortunately, little attention has been paid to the corrosion behavior of Q235 mild steel in seawater using the EN technique, especially the effect of the dissolved oxygen content on the corrosion mechanism.

The aim of the present work is to study the corrosion behavior of Q235 mild steel in artificial seawater using both EIS and EN techniques, especially to evaluate the effect of dissolved oxygen content on the corrosion rate and mechanism. Additionally, a new parameter is proposed from the wavelet transformation analysis of the EN data and is applied to in-situ monitor the corrosion resistance, which agrees well with the EIS measurements during the initial immersion time.

2. EXPERIMENTAL

An aggressive electrolyte was prepared from analytical grade chemicals and deionized water. The chemical composition of the artificial seawater is listed in **Table 1**. A classic glass electrolysis cell with an inlet and outlet to maintain the dissolved oxygen concentration in the artificial seawater was used. Pure N_2 was initially blown into the electrolyte for over 2 h to obtain an oxygen-free solution, and then a mixture of O_2 and N_2 was employed for at least 4 h before the electrochemical measurements. The dissolved oxygen concentration was controlled by mixing different ratios (v/v) of O_2 and N_2 using an accurate flowmeter, and the dissolved oxygen concentration was maintained at 50, 100, 200 and 500 μg/L under these experimental conditions. A conventional three electrode system

was employed to perform the electrochemical measurements. Q235 mild steel substrates with exposure area of 0.50 cm2 were used as working electrodes to investigate the effect of dissolved oxygen concentration in artificial seawater on the corrosion behavior of Q235 mild steel during the initial 7 days. Before each experiment, the Q235 mild steel substrate was polished to a mirror-like finish using different grits of emery paper and alumina powder, cleaned with deionized water, rinsed with acetone and later dried with N_2. Platinum foil and a saturated calomel electrode (SCE) were used as the counter and reference electrodes, respectively.

Table 1. Detailed chemical composition of artificial seawater.

Component	NaCl	$CaCl_2$	$MgCl_2.6H_20$	Na_2SO_4	$NaHC0_3$	KCl
wt.%	2.52	0.24	0.65	0.58	0.15	0.08

EIS measurements were conducted using an impedance measurement unit (PARSTAT 2273, Advanced Electrochemical System) in a frequency range from 100,000 Hz down to 0.01 Hz at the open circuit potential (E_{ocp}). The sine voltage perturbation was adjusted to 5 mV in amplitude. Z-view software was used to fit the EIS data. EN data of the Q235 mild steel corrosion in artificial seawater containing different concentrations of dissolved oxygen during the initial 7 days were recorded with a commercial PowerLab coupled to a GP Amp device (ADInstruments Pty Ltd., Australia) at a sampling rate of 4 Hz. All electrochemical tests were performed in a quiescent solution and the experimental device was shielded in a Faradaic cage. Each test was performed at least three times and the average values were reported.

The morphologies of the Q235 mild steel surfaces after corrosion in artificial seawater containing different concentrations of dissolved oxygen for one day were observed with scanning electron microscope (SEM, Hitachi SU80) at a 5000X magnification.

3. RESULTS AND DISCUSSION

3.1 EIS measurements

Fig.1- Fig.4 displays the EIS diagrams for Q235 mild steel corrosion in artificial seawater containing different concentrations of dissolved oxygen at different immersion times. Both the dissolved oxygen concentration and immersion time have a significant effect on the corrosion behavior of Q235 mild steel corrosion in artificial seawater. In most cases, the EIS diagrams show the largest impedance when immersed in artificial seawater for one day. After that, the impedance decreases with prolonged immersion time for different dissolved oxygen concentrations. Moreover, the impedance also decreases with an increasing dissolved oxygen concentration from 50 μg/L to 500 μg/L in artificial seawater, which may be related to the large corrosion rate.

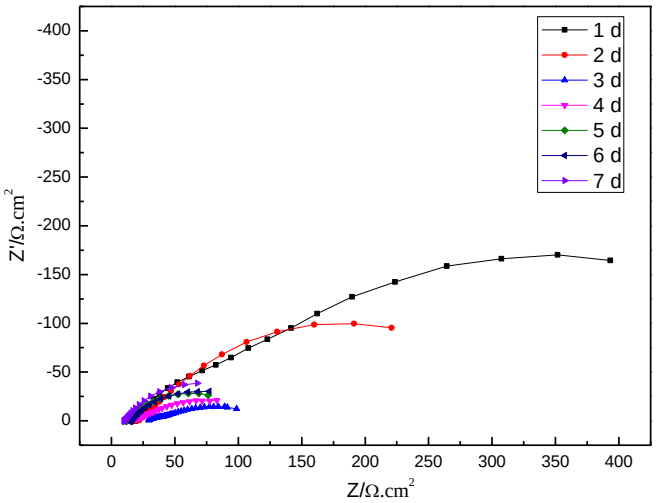

Figure 1. EIS plots of Q235 mild steel corrosion in artificial seawater containing 50 μg/L dissolved oxygen at different immersion time.

Generally, the features of the EIS diagrams, including the numbers for the phase angle peak and impedance slopes in the Bode plot and the number of capacitances in the Nyquist plot, can be used to explore the time-constant numbers in the EIS diagrams through a method proposed by Wit [21,22]. It can be deduced that for different dissolved oxygen concentrations and immersion times, the EIS diagrams all contain two time constants. The one located in the high frequency domain corresponds to the charge transfer process during Q235 mild steel corrosion, whereas the other, which is located in the middle frequency domain can be related to a oxide film formed on the Q235 mild steel surface.

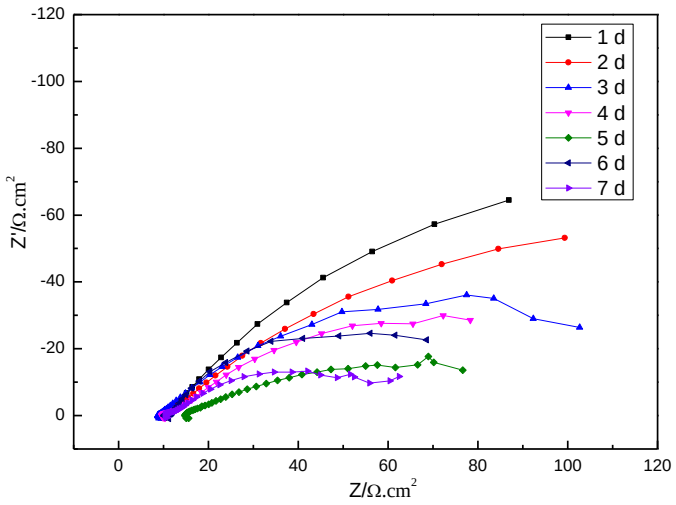

Figure 2. EIS plots of Q235 mild steel corrosion in artificial seawater containing 100 μg/L dissolved oxygen at different immersion time.

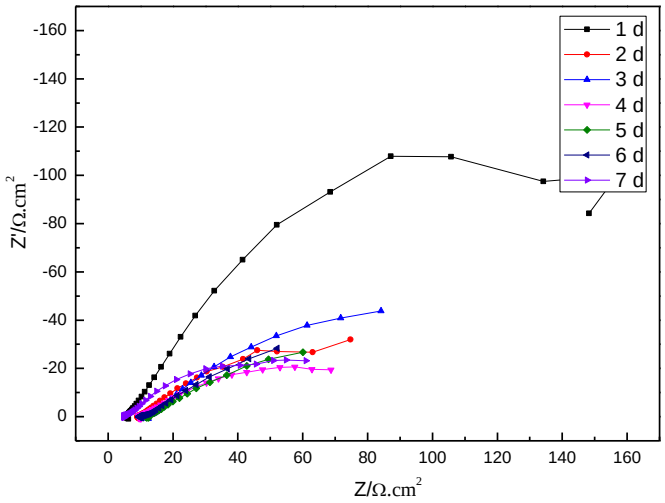

Figure 3. EIS plots of Q235 mild steel corrosion in artificial seawater containing 200 μg/L dissolved oxygen at different immersion time.

An inspection of Fig.1- Fig.4, clearly shows that the centers of the two capacitances are below the real axis, which is known as "frequency dispersion" and is caused by the surface roughness and heterogeneities of the Q235 mild steel [23]. Thus, the ideal capacitance C is replaced by a constant phase element (CPE) when simulating the EIS data. The impedance of the CPE can be calculated as follows [24-26]:

$$Z_{CPE} = \frac{1}{Y_0(j\omega)^n} \quad (1)$$

where Y_0 is the magnitude of the CPE, ω corresponds to the angular frequency, and n is the phase and represents the Q235 mild steel surface heterogeneities in this study.

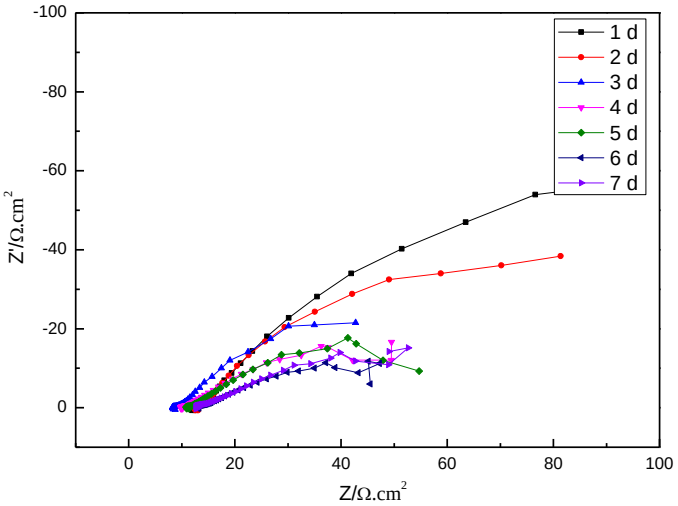

Figure 4. EIS plots of Q235 mild steel corrosion in artificial seawater containing 500 μg/L dissolved oxygen at different immersion time.

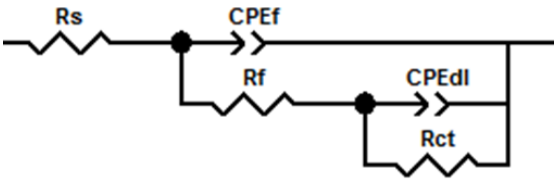

Figure 5. EEC used for simulating the impedance spectra.

Therefore, to further analyze the Q235 mild steel corrosion in artificial seawater containing different dissolved oxygen concentrations at different immersion time, an equivalent electrical circuit (EEC) as shown in Fig.5, is employed to quantitatively analyze the EIS data by using Z-view software. In this equivalent electrical circuit, R_s is assigned to the solution resistance, CPE_f represents the film capacitance, $R_f$is the resistance of the oxide film formed on Q235 mild steel during its corrosion process, CPE_{dl} corresponds to the double layer capacitance and R_{ct} is the charge transfer resistance. The fitted results are summarized in Tables 1-4. When the dissolved oxygen concentration is 50 μg/L, the value of R_{ct} decreases from 586 $\Omega.cm^2$ to 96.1 $\Omega.cm^2$ with a prolonged immersion time from 1 day to 7 days. When increasing the dissolved oxygen concentration from 50 μg/L to 500 μg/L in the artificial seawater, the value of R_{ct} decreased from 586 $\Omega.cm^2$ to 189 $\Omega.cm^2$. Moreover, the value of R_f also shows the same variation trend in which it decreases with increasing the dissolved oxygen concentration and immersion time. The reduction of R_{ct} and R_f can be related to the loose and porous oxide film; the film cannot inhibit the penetration of corrosive ions and dissolved oxygen to the Q235 mild steel surface, thus causing the much more serious corrosion of Q235 mild steel in the artificial seawater.

Table 1. EIS analyzed results for Q235 mild steel corrosion in artificial seawater containing 50 μg/L dissolved O_2 at different immersion time.

Time/d	R_f $\Omega.cm^2$	CPE_f Ω^{-1} s^n cm^{-2}	n_f	R_{ct} $\Omega.cm^2$	CPE_{dl} Ω^{-1} s^n cm^{-2}	n_{dl}
1	142	163	0.98	586	28.3	0.85
2	65.3	224	0.98	294	49.7	0.86
3	15.1	316	0.98	98.6	79.9	0.81
4	10.8	347	0.96	72.5	83.2	0.83
5	12.2	334	0.97	79.3	86.5	0.84
6	11.5	341	0.96	88.6	82.9	0.81
7	14.7	328	0.97	96.1	76.4	0.81

Table 2. EIS analyzed results for Q235 mild steel corrosion in artificial seawater containing 100 μg/L dissolved O_2 at different immersion time.

Time/d	R_f $\Omega.cm^2$	CPE_f Ω^{-1} s^n cm^{-2}	n_f	R_{ct} $\Omega.cm^2$	CPE_{dl} Ω^{-1} s^n cm^{-2}	n_{dl}
1	29	413	0.91	389	42.5	0.80
2	9.4	425	0.95	237	99.8	0.86
3	6.5	276	0.93	96	138	0.84
4	2.8	289	0.91	76	92.9	0.83
5	0.9	171	0.90	90.6	59.7	0.84
6	1.7	424	0.91	75.5	27.7	0.82
7	2.1	157	0.92	89.5	35.8	0.84

Table 3. EIS analyzed results for Q235 mild steel corrosion in artificial seawater containing 200 μg/L dissolved O_2 at different immersion time.

Time/d	R_f $\Omega.cm^2$	CPE_f Ω^{-1} s^n cm^{-2}	n_f	R_{ct} $\Omega.cm^2$	CPE_{dl} Ω^{-1} s^n cm^{-2}	n_{dl}
1	7.3	261	0.90	267	239	0.83
2	1.4	376	0.94	131	240	0.85
3	2.9	368	0.98	86	605	0.81
4	1.8	289	0.88	97	811	0.80
5	3.7	354	0.93	72	331	0.83
6	3.2	622	0.92	85	191	0.80
7	1.3	532	0.93	71	343	0.83

Table 4. EIS analyzed results for Q235 mild steel corrosion in artificial seawater containing 500 μg/L dissolved O_2 at different immersion time.

Time/d	R_f $\Omega.cm^2$	CPE_f Ω^{-1} s^n cm^{-2}	n_f	R_{ct} $\Omega.cm^2$	CPE_{dl} Ω^{-1} s^n cm^{-2}	n_{dl}
1	3.1	384	0.89	189	68	0.86
2	2.9	373	0.94	102	108	0.88
3	2.1	604	0.96	87	210	0.89
4	2.9	287	0.93	80	90	0.88
5	2.0	385	0.93	71	101	0.85
6	4.8	239	0.91	75	184	0.82
7	2.8	468	0.95	56	328	0.88

3.2 EN analysis

Fig.6-9 shows the potential EN data during Q235 mild steel corrosion in artificial seawater containing different concentrations of dissolved oxygen at different immersion times. Generally, the recorded electrochemical potential data are composed of the electrochemical potential noise and corrosion potential. The electrochemical potential noise and corrosion potential are assigned to the spontaneous fluctuation and the mean value, respectively [27]. As seen from Fig 6(a), a small potential oscillation amplitude can be observed for Q235 mild steel corrosion in artificial seawater containing 50 μg/L dissolved oxygen when immersed for one day, which may indicate that weak localized corrosion occurs on the Q235 mild steel surface at the initial immersion time. It can also be seen that the EN curves exhibit different characteristics at different dissolved oxygen concentrations and immersion times. Under a certain dissolved oxygen concentration, it is apparent that the corrosion potential shifts in the positive direction with prolonged immersion time, which may be due to the formation of an oxide film on the Q235 mild steel surface.

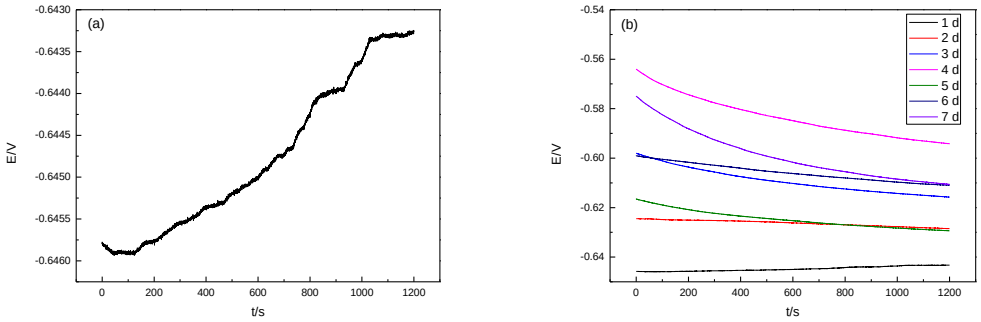

Figure 6. Electrochemical potential noise of Q235 mild steel corrosion in artificial seawater containing 50 μg/L dissolved oxygen at different immersion time. (a) the first day; (b) the initial one week.

To give deep insights into the EN features and the corrosion behavior of the Q235 mild steel in the artificial seawater containing different concentrations of dissolved oxygen at different immersion times, a fast wavelet transformation (FWT) was employed to quantitatively analyze the electrochemical potential noise data of the initial 5120 points. The theoretical algorithm of FWT has been introduced in previous studies [28,29]. According to the FWT analysis algorithm (Figure 10), a given time record $x_i(t)(i = 1,2,\dots,N)$ can be expressed using a linear combinations of basis functions $\emptyset_{j,k}$ and $\varphi_{j,k}$ and amplitude coefficients of each function $S_{J,k}$, $D_{J,k}$,…, $D_{l,k}$

$$x(t) \approx \sum_k S_{J,k}\,\emptyset_{J,k}(t) + \sum_k D_{J,k}\,\varphi_{J,k}(t) + \sum_k D_{J-1,k}\,\varphi_{J-1,k}(t) + \cdots + \sum_k D_{1,k}\,\varphi_{1,k}(t) \quad (2)$$

$$S_{J,k} = \int x(t)\emptyset^*_{J,k}(t)dt \quad (3)$$

$$D_{l,k} = \int x(t)\varphi^*_{l,k}(t)dt \quad (4)$$

Where $\emptyset^*_{J,k}$ and $\varphi^*_{l,k}$ are the complex conjugate of the basis functions father wavelet $\emptyset(t)$ and mother wavelet $\varphi(t)$, and they are the basis for this decomposition through translating and scaling using the following equations:

$$\emptyset_{J,k}(t) = 2^{-J/2}\emptyset(2^{-J}t - k) = 2^{-J/2}\emptyset(\frac{t-2^J k}{2^J}) \quad (5)$$

$$\varphi_{J,k}(t) = 2^{-l/2}\varphi(2^{-l}t - k) = 2^{-l/2}\varphi(\frac{t-2^l k}{2^l}) \quad (6)$$

Where $k = 1,2,\ldots,N/2$, N is the number of the given time record. $l = 1,2,\ldots,J$, J is often a small natural number. Meanwhile, 2^l corresponds to the scale factor and $2^l k$ is related to the translation parameter.

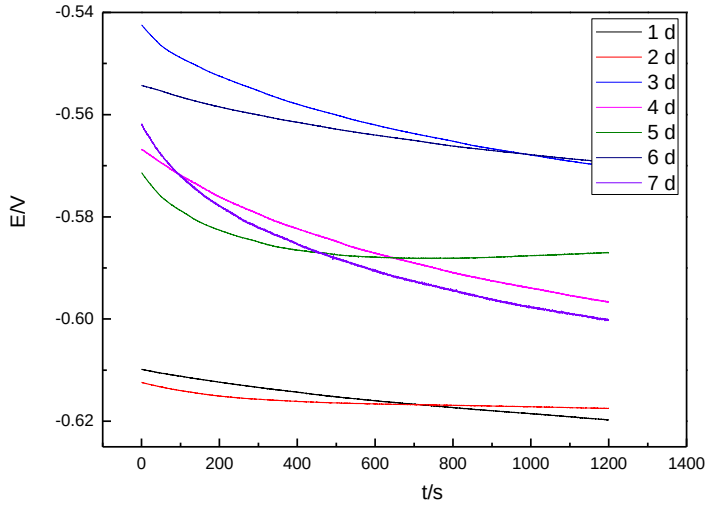

Figure 7. Electrochemical potential noise of Q235 mild steel corrosion in artificial seawater containing 100 μg/L dissolved oxygen at different immersion time.

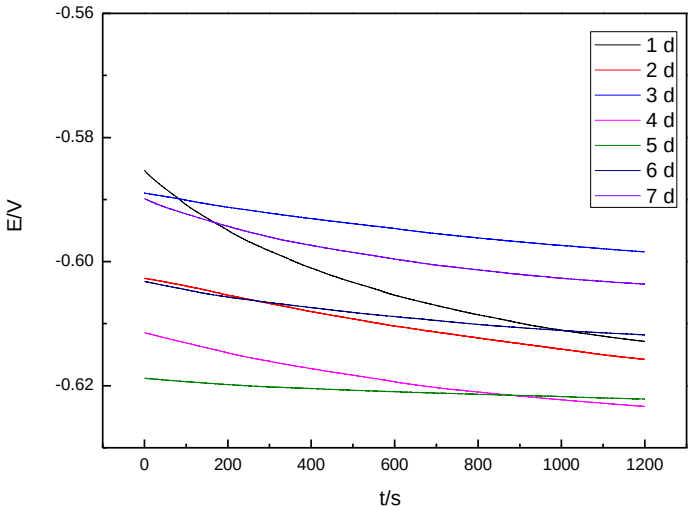

Figure 8. Electrochemical potential noise of Q235 mild steel corrosion in artificial seawater containing 200 μg/L dissolved oxygen at different immersion time.

The energy accumulated at different timescales for the Q235 mild steel corrosion in artificial seawater containing different concentrations of dissolved oxygen at different immersion times. It is known that different timescales in the RP-EDPs correspond to different corrosion events, where small timescales are assigned to relatively fast corrosion events, such as metastable pitting in a high

frequency range, and large timescales are ascribed to a slow process, such as general corrosion in the low frequency domain [30]. It has been concluded in previous researches that the RP-EDPs can be rationally classified into three parts [31-33]: (1) region A, which is located between D_1 and D_3 in the small timescales corresponds to the fast process, such as metastable pitting, (2) region B located between D_3 and D_6 in the middle timescales is assigned to the pitting development, and (3) region C located between D_6 and D_8 in the large timescales, characterizes a relatively slow process, such as a diffusion process. When the dissolved oxygen concentration is 50 μg/L, the main accumulated relative energy domain transfers from the smaller timescales to the larger timescales with different immersion times, indicating a predominant diffusion process of the corrosive species onto the Q235 mild steel surface at the initial immersion times. When the dissolved oxygen concentration is increased to 500 μg/L, the relative energy mainly accumulates in the large timescales during the whole immersion time, which suggests a predominance of localized corrosion at high dissolved oxygen concentrations.

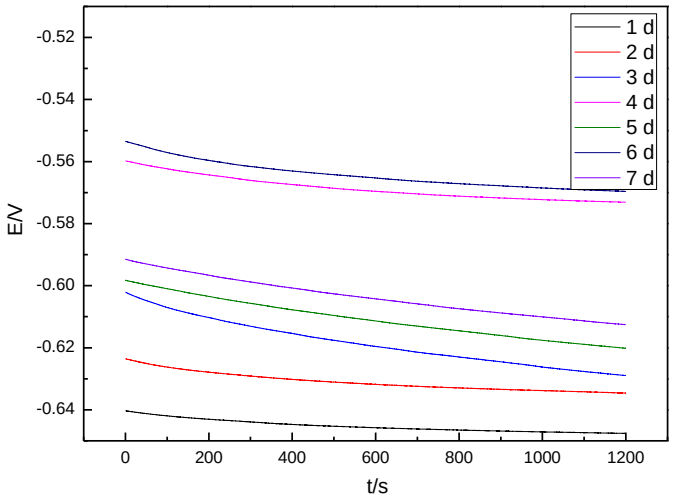

Figure 9. Electrochemical potential noise of Q235 mild steel corrosion in artificial seawater containing 500 μg/L dissolved oxygen at different immersion time.

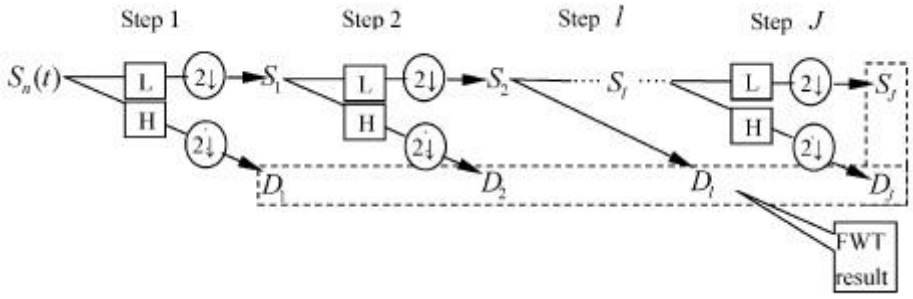

Figure 10. Theoretical algorithm scheme of the fast wavelet transform.

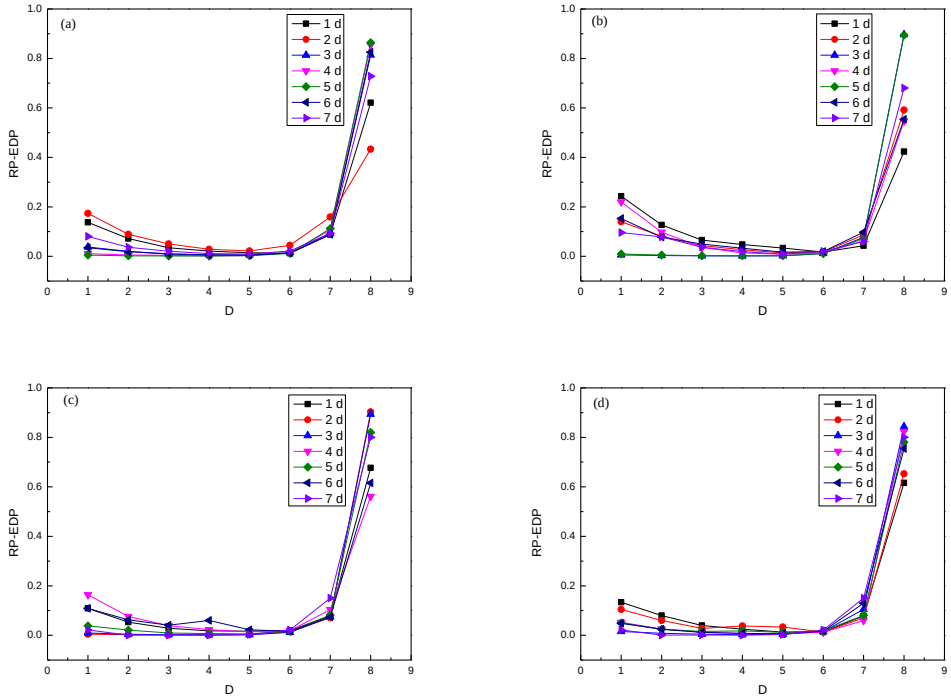

Figure 11. RP-EDPs generated during Q235 mild steel corrosion in artificial seawater containing different concentration of dissolved oxygen at different immersion time. (a) 50 μg/L; (b) 100 μg/L; (c) 200 μg/L; (d) 500 μg/L.

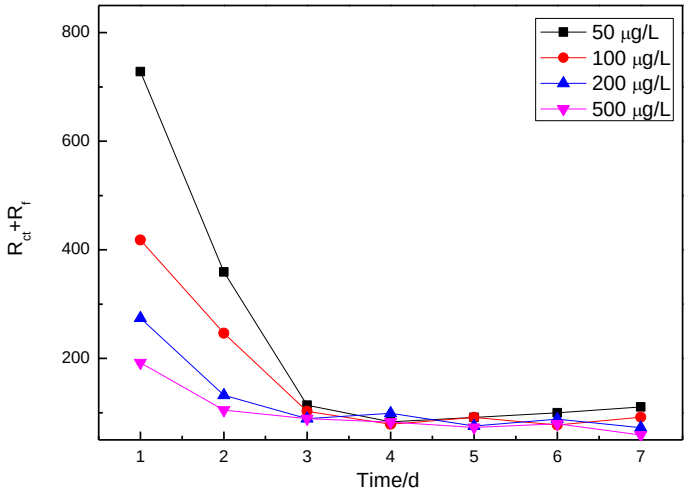

Figure 12. Dependence of $R_{ct}+R_f$ on dissolved oxygen concentrations.

From Figure 10, it is obvious that the discrete signal $x_i(t)(i = 1,2, \dots, N)$ is initially decomposed into two sets of coefficients through high-pass filter (H) and low-pass filter (L): one coefficient set $D_l = (D_1, D_2, \dots, D_J)$ contains the local information of the original signal and the other smooth coefficient set $S_l = (S_1, S_2, \dots, S_J)$ encodes the information about the general trend of the original signal. After filtering, the outputs are down-sampled (2 ↓) and one of every two consecutive sample of the filtered components has been deleted. At last, both the smooth coefficients S_l and detail

coefficients D_l are saved, which is named a crystal and associated with the features of the original signal, respectively [28,29].

Therefore, the overall energy (E) of the electrochemical potential noise in our experiment was calculated as follows:

$$E = \sum_{n=1}^{N} S_n^2 (n = 1,2,..., N, N = 5120) \qquad (7)$$

Then, the fraction of energy related to each crystal (D and S) can be calculated using the following equations:

$$E_l^D = \frac{1}{E} \sum_{k=1}^{N/2^l} D_{l,k}^2 (l = 1,2,..., J, J = 8) \qquad (8)$$

$$E_J^S = \frac{1}{E} \sum_{k=1}^{N/2^l} S_{J,k}^2 (l = 1,2,..., J) \qquad (9)$$

Thus, the overall energy E can also be expressed as follows due to the orthogonal nature of the employed wavelets:

$$E = E_J^S + \sum_{l=1}^{J} E_l^D \qquad (10)$$

Based on the above analysis, the energy distribution plot (EDP) can be obtained by plotting the relative energy versus the corresponding crystal. Moreover, after removing the energy contribution of S8 crystal from the total energy of the electrochemical potential noise, a re-plotted EDP can be gained and defined as RP-EDP. The RP-EDPs of Q235 mild steel corrosion in the artificial seawater containing different concentrations of dissolved oxygen at different immersion times are displayed inFig.11.

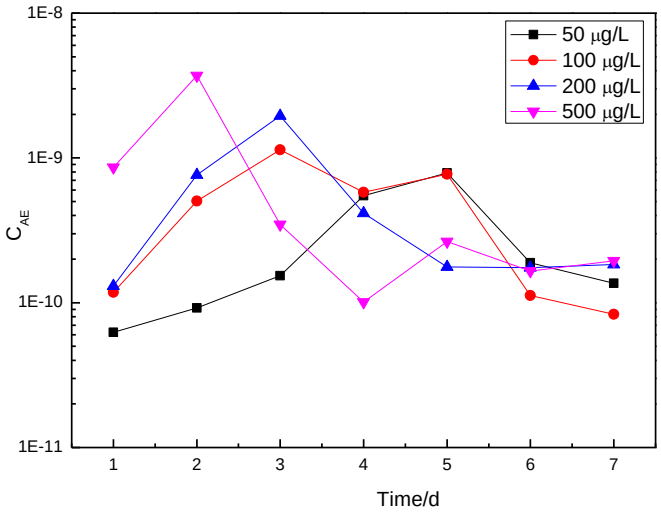

Figure 13. Dependence of C_{AE} on dissolved oxygen concentrations.

As seen from Fig.11, the RP-EDP plots are very similar for Q235 mild steel corrosion in the artificial seawater containing different concentrations of dissolved oxygen. Meanwhile, the relative energies all accumulated in the large timescales at different immersion times. Thus, it is still difficult

to establish the quantitative relationship between the EN features and the corrosion rate during Q235 mild steel corrosion in artificial seawater containing different concentrations of dissolved oxygen at different immersion times. Therefore, a new electrochemical parameter C_{AE}, which represents the electrochemical reaction rate, is calculated from the FWT analysis of EN data using the following equation [31],

$$C_{AE} = E_{d1} + E_{d2} + E_{d3} + E_{d4} + E_{d5} + E_{d6} \quad (11)$$

where $E_{d1} + E_{d2} + E_{d3}$ is the energy related to the pitting nucleation process in region A, and $E_{d4} + E_{d5} + E_{d6}$ is the energy corresponding to the pitting growth process in region B.

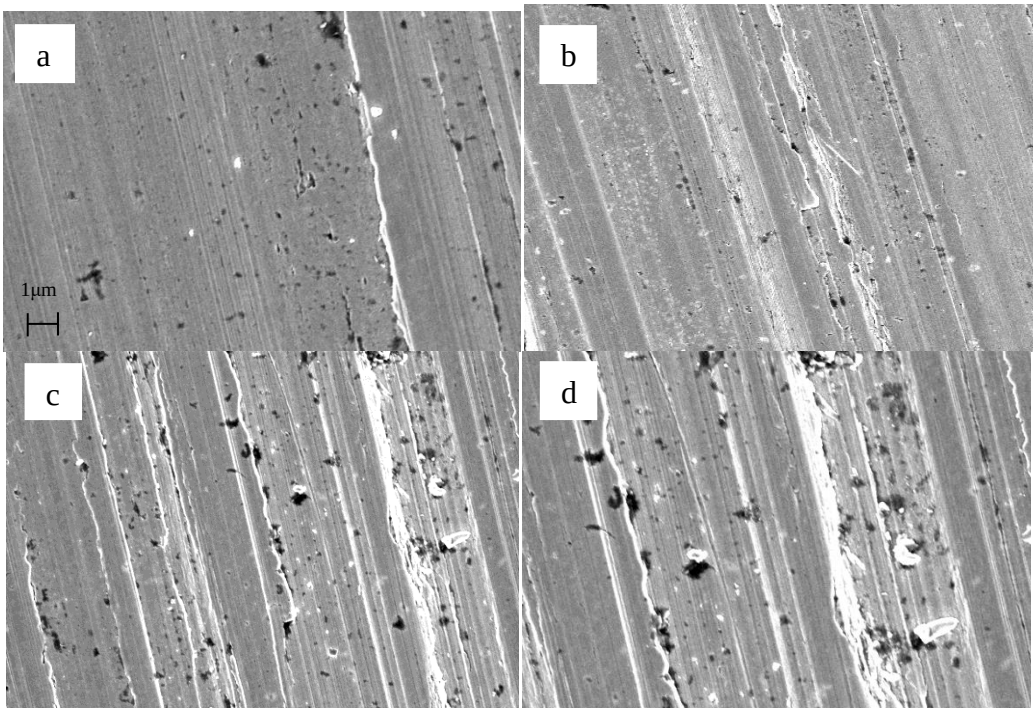

Figure 14. SEM images of Q235 mild steel after corroded in artificial seawater containing different concentration of dissolved oxygen for one day. (a) 50 μg/L; (b) 100 μg/L; (c) 200 μg/L; (d) 500 μg/L.

The dependence of the sum of the charge transfer resistance R_{ct} and film resistance R_f on the dissolved oxygen concentration is shown in Fig.12. It is clear that for different dissolved oxygen concentrations, the sum of the charge transfer resistance R_{ct} and film resistance R_f decreases with increasing immersion time. The sum of R_{ct} and R_f exhibits large values at low dissolved oxygen concentrations. Furthermore, the C_{AE} versus the dissolved oxygen concentration is plotted in Fig.13. The value of C_{AE} initially increases with immersion time and then decreases with prolonged testing time. Interestingly, with an increase in the dissolved oxygen concentration, short time is needed for the C_{AE} to reach its maximum value. Moreover, the sum of R_{ct} and R_f show the similar variation trend with C_{AE} after long immersion times.

Fig.14 shows the Q235 mild steel surface morphologies after corrosion in artificial seawater containing different concentrations of dissolved oxygen for one day. It is clear that the Q235 mild steel surface is damaged after immersion in artificial seawater containing different concentrations of dissolved oxygen for one day. In addition to the scratches originating from the polishing process, different sizes of pits can also be observed on the Q235 mild steel surface. Moreover, with increasing dissolved oxygen concentration, the quantity and diameter of the formed pits increase significantly, suggesting an enhanced pitting process when exposed to high dissolved oxygen concentration at the initial immersion time. This observation is in good accordance with that of the variation trend of C_{AE} at different dissolved oxygen concentrations.

The dissolution of mild steel in chloride solution can be expressed with the following equations [34]:

$$Fe \rightarrow Fe^{2+} + 2e^{-} \quad (12)$$

$$O_2 + 2H_2O + 4e^{-} \rightarrow 4OH^{-} \quad (13)$$

$$Fe^{2+} + 2OH^{-} \rightarrow Fe(OH)_2 \quad (14)$$

In the presence of dissolved oxygen, the formed $Fe(OH)_2$ will further convert to FeOOH or be reduced to Fe_3O_4,

$$4Fe(OH)_2 + O_2 + 2H_2O \rightarrow 4Fe(OH)_3 \quad (15)$$

$$Fe(OH)_3 \rightarrow FeOOH + H_2O \quad (16)$$

$$6Fe(OH)_2 + O_2 \rightarrow 2Fe_3O_4 + 6H_2O \quad (17)$$

Gradually, part of FeOOH will be changed to Fe_2O_3 through a dehydration process:

$$2FeOOH \rightarrow Fe_2O_3 + H_2O \quad (18)$$

$$Fe^{2+} + 2Cl^{-} \rightarrow FeCl_2 \quad (19)$$

$$FeCl_2 + 2H_2O \rightarrow Fe(OH)_2 + 2HCl \quad (20)$$

It has been reported that carbon steel reaches a pseudopassivation state under the effect of dissolved oxygen during the initial immersion period [35]. However, this pseudopassivation state is not steady and can be easily destroyed by a complexing dissolution of the oxide film in the presence of chloride [36]. The chloride also makes the formed oxide film porous, which is beneficial for the diffusion of dissolved oxygen to the Q235 mild steel substrate. Consequently, the sum of the charge transfer resistance R_{ct} and film resistance R_f decreases with immersion time at the initial testing time (Fig.12). Furthermore, due to the potential difference between the formed oxide film and bare Q235 mild steel substrate, the localized corrosion take place (Fig.14). Xue [19] suggested that the occurrence of localized corrosion on Q235 mild steel was related to both the presence of chloride and the concentration of dissolved oxygen. As a result, some small pits will be formed at the active sites on the Q235 mild steel surface (Fig.14). Due to the hydrolysis process of ferrous ions in the small pits, the pH value of this micro domain decreases, which will inevitably accelerate the active dissolution of the Q235 mild steel and cause an increase in the C_{AE} value (Fig.13).

After a certain reaction time, an increasing number of corrosion products (Fe_2O_3 and/or Fe_3O_4) are formed under the synergistic effect between the chloride and dissolved oxygen on the Q235 mild steel surface. The formed protective films will significantly block the channels for the penetration of chloride and dissolved oxygen to the reaction interface. Therefore, the sum of charge transfer resistance R_{ct} and film resistance R_f reaches a relatively stable value (Fig.12). Moreover, when these

protective films fully cover the Q235 mild steel surface, the Q235 mild steel surface reaches a relatively homogeneous state and the localized corrosion will convert to uniform corrosion. Then the C_{AE} value decreases with prolonged testing time. With a high dissolved oxygen concentration, the cathodic reaction rate can be enhanced and results in a small corrosion resistance (Fig.12). Compared to the low dissolved oxygen concentration, the oxide film will be formed much more quickly under a high dissolved oxygen concentration, which will considerably reduce the time to reach equilibrium between the dissolution and reparation of the oxide film. Consequently, C_{AE} reaches its the maximum value more quickly in the presence of a high dissolved oxygen concentration (Fig.13).

4. CONCLUSIONS

The effect of the dissolved oxygen concentration and immersion time on the corrosion behavior of Q235 mild steel in artificial seawater was studied using EIS, EN and SEM techniques. EIS results reveal that the sum of the charge transfer resistance and film resistance decreases with immersion time and that the sum of the charge transfer resistance and film resistance possesses large values with low dissolved oxygen concentrations. A new electrochemical parameter C_{AE}, which represents the electrochemical reaction rate, is proposed and applied to further study the effect of dissolved oxygen concentration on the corrosion resistance and corrosion mechanism. The value of C_{AE} first increases at the initial immersion times and later decreases with prolonged testing times. The time for C_{AE} to reach the maximum value was shortened in the presence of a large dissolved oxygen concentration, which may be related to an enhanced cathodic reaction rate. At the same time, the characteristics of Q235 mild steel surface morphologies match well with the variation trend of C_{AE} at different dissolved oxygen concentrations. Thus, the new parameter C_{AE} can serve as a new criterion to monitor the corrosion resistance and surface morphology in situ.

ACKNOWLEDGEMENTS
The authors wish to acknowledge the Natural Science Foundation of Shandong Province (ZR2019QEM003, 2019KJC020), the Project of Focus on Research and Development Plan in Shandong Province (2019GSF111048), the Major Project of Binzhou University (2019ZD02), and the Scientific Research Fund of Binzhou University (BZXYLG1904).

References

1. S. Ralkhal, T. Shahrabi and B. Ramezanzadeh, *Constr. Build. Mater*., 222 (2019) 400.
2. B. Thirumalairaj and M. Jaganathan, *Egypt. J. Petrol*., 25 (2016) 423.
3. D. Daoud, T. Douadi, H. Hamani, S. Chafaa and M. Al-Noaimi, *Corros. Sci.*, 94 (2015) 21.
4. Yuhua Gao, L. Ward, Linhua Fan, Haihua Li and Zhenfa Liu, *J. Mol. Liq*., 294 (2019) 111634.
5. M.A. Amin, S.S. Abd El-Rehim, E.E.F. El-Sherbini and R.S. Bayoumi, *Electrochim. Acta*, 52 (2007) 3588.
6. S.D. Deng and X.H. Li, Corros. Sci., 64 (2012) 253.
7. M.A. Hegazy, A.M. Badawi, S.S. Abd El Rehim and W.M. Kamel, *Corros. Sci.*, 69 (2013) 110.

8. Z. Salarvand, M. Amirnasr, M. Talebian, K. Raeissi and S. Meghdadi, *Corros. Sci*., 114 (2017) 133.
9. M. Mobin and M. Rizvi, *Carbohyd. Polym*., 160 (2017) 172.
10. G.L.F. Mendonca, S.N. Costa, V.N. Freire, P.N.S. Casciano, A.N. Correia and Pedro de Lima-Neto, *Corros. Sci.*, 115 (2017) 41.
11. A. Ghazoui, N. Benchat, F. El-Hajjaji, M. Taleb, Z. Rais, R. Saddik, A. Elaatiaoui and B. Hammouti, *J. Alloy. Compd*., 693 (2017) 510.
12. Zhihua Tao, Shengtao Zhang, Weihua Li and Baorong Hou, *Corros. Sci.*, 51 (2009) 2588.
13. M. Bouanis, M. Tourabi, A. Nyassi, A. Zarrouk, C. Jama and F. Bentiss, *Appl. Surf. Sci*., 389 (2016) 952.
14. Weiwei Cheng, Shengyun Luo and Yu Chen, *Int. J. Electrochem. Sci*., 14 (2019) 4254.
15. D.M. Ortega-Toledo, J.G. Gonzalez-Rodriguez, M. Casales, L. Martinez and A. Martinez-Villafa, *Corros. Sci.*, 53 (2011) 3780.
16. G. Suresh and U.K. Mudali, *Corrosion*, 70 (2014) 283.
17. H. Ashassi-Sorkhabi, D. Seifzadeh and M. Raghibi-Boroujeni, *Arab. J. Chem.*, 9 (2016) S1320.
18. Beibei Zhang, Jianzhang Wang, Junya Yuan and Fengyuan Yan, *Friction*, 7 (2019) 444.
19. F. Xue, X. Wei, J. Dong, C. Wang and W. Ke, *J. Mater. Sci. Technol*., 35 (2019) 596.
20. F. Xue, X. Wei, J. Dong, I.N. Etim, C.G. Wang and W. Ke, *J. Mater. Sci. Technol*., 34 (2018) 1349.
21. D.H. van der Weijde, E.P.M. van Westing and J.H.W.de Wit, *Corros. Sci*., 36 (1994) 643.
22. P. Campestrini, E.P.M van Westing and J.H.W de Wit, *Electrochim. Acta*, 46 (2001) 2631.
23. R. Solmaz, G. Kardas, M. Culha, B. Yazici and M. Erbil. *Electrochim. Acta*, 53 (2008) 5941.
24. A. Popova, E. Sokolova, S. Raicheva and M. Christov, *Corros. Sci*., 45 (2003) 33.
25. N.D. Nam, Q.V. Bui, M. Mathesh, M.Y.J. Tan and M. Forsyth, *Corros. Sci*., 76 (2013) 257.
26. I. Ahamad, R. Prasad and M. Quraishi, *Mater. Chem. Phys*., 124 (2010) 1155.
27. D. Seifzadeh, H. Basharnavaz and A. Bezaatpour, *Mater. Chem. Phys*., 138 (2013) 794.
28. X.Q. Huang, Y. Chen, T.W. Fu, Z. Zhang and J.Q. Zhang, *J. Electrochem. Soc*., 160 (2013) D530.
29. C. Cai, Z. Zhang, F.H. Cao, Z.N. Gao, J.Q. Zhang and C.N. Cao, *J. Electroana. Chem*., 578 (2005) 143
30. S.M. Hoseinieh, A.M. Homborg, T. Shahrabi, J.M.C. Mol and B. Ramezanzadeh, *Electrochim. Acta*, 217 (2016) 226.
31. Y. Chen, Z.N. Yang, Y.W. Liu, H.H. Zhang, J.Y. Yin, Y. Xie and Z. Zhang, *J. Taiwan. Inst. Chem. E*., 80 (2017) 908.
32. Y.W. Liu, Y. Chen, X.H. Chen, Z.N. Yang, Y. Xie and Z. Zhang, *J. Alloy. Compd.*, 758 (2018) 184.
33. Y. Chen, X.H. Chen, Y.W. Liu, H.H. Zhang, Y. Xie, Z.N. Yang and Z. Zhang, *J. Chem. Thermodyn*., 126 (2018) 147.
34. Y.G. Su, B.L. Fang, P.H. Lv, C.W. Du, D. Ding, B. Cao, L. Liu and Z.Y. Liu, *Corros. Sci. Prot. Technol.*, 30 (2018) 279 (in chinses).
35. J. Han, D. Young, H. Colijn, A. Tripathi and S. Nesic, *Ind. Eng. Chem. Res*., 48 (2009) 6296.
36. J.H. Wang, C.C. Su and Z. Szklarska-Smialowska, *Corrosion*, 44 (1988) 732.